JMEPEG (2015) 24:2885–2897
DOI: 10.1007/s11665-015-1571-5

1059-9495/$19.00

Corrosion Behavior of Field-Exposed 7A04 Aluminum Alloy in the Xisha Tropical Marine Atmosphere

Z.Y. Cui, X.G. Li, C. Man, K. Xiao, C.F. Dong, X. Wang, and Z.Y. Liu

(Submitted February 9, 2015; in revised form April 14, 2015; published online June 23, 2015)

Atmospheric corrosion behavior of 7A04 aluminum alloy exposed to a tropical marine environment for 4 years was investigated by weight loss test, morphology observation, and electrochemical impendence spectroscopy (EIS). The results showed that the weight loss of 7A04 alloy in the log-log coordinates can be approximately fitted with two liner segments, in which the slope value of the second segment is significantly lower than that of the first segment. This was mainly attributed to the protectiveness of the corrosion product layer formed on the specimen exposed for 12 and 24 months, which was further confirmed by the EIS results. Corrosion rate presented a significant fluctuation during the exposure test which is due to the deterioration effect caused by chloride ions and time of wetness and the stabilization process of the corrosion product layer. Intergranular corrosion occurred on the 7A04 alloy and then transformed into exfoliation corrosion because of the synergetic effect of the hydrogen-assisted crack initiation and the wedge effect-induced matrix delamination.

Keywords aluminum alloy, atmospheric corrosion, exfoliation corrosion

1. Introduction

Atmospheric corrosion is one of the leading causes of structural damage to aluminum alloys, which have been extensively used as structural materials in the aircraft and aerospace industries (Ref 1, 2). Of particular importance is pitting and intergranular corrosion, which can develop into fatigue cracks, stress corrosion cracks, or exfoliation (Ref 3). Therefore, it is of interest to understand how corrosion propagates in susceptible aluminum alloys in tropical marine atmosphere where the aircraft sometimes executes flying missions.

There have been some field exposure studies that investigate the atmospheric corrosion behavior of aluminum alloys in various environments (Ref 4–10). Among them, pitting corrosion (Ref 4–8), intergranular corrosion (Ref 6, 9, 10), exfoliation corrosion (Ref 9, 10), and stress corrosion (Ref 6) are all detected on several kinds of aluminum alloys. It was reported that the forged truck wheels made of 2024-T4 exfoliated severely in only 1 or 2 years in the northern states of United States, where deicing salts were used on the highways during the winter months (Ref 11). Sun (Ref 9) conducted a field exposure test on 2024 and 7075 aluminum alloys in urban, coastal, and industrial environments for 20 years. The results showed that the relationship between weight loss and exposure time obeyed the power function. Exfoliation corrosion occurred on extruded 2024 and 7075 in coastal and industrial atmospheres, leading to great mechanical property degradation. Wang (Ref 6) investigated the atmospheric corrosion of 2024-T3 alloy exposed to salt lake environment and suggested that the mass loss increased at a high rate in the first 2 years, and tended to stabilize over time. Besides the pitting corrosion and intergranular corrosion, stress corrosion cracks were also observed on the 2024-T3 alloys. Despite all this, the corrosion kinetics and mechanism of aluminum alloys still needs to be well understood.

Generally, corrosion resistance of Al alloy during long-term exposure is attributed to the formation of a layer of oxide film or corrosion product composed of $Al(OH)_3$ on its surface (Ref 12). This layer would control the diffusion of the reaction species and inhibit the corrosion process. The relationship between corrosion product protectiveness and weight loss of some other metals has been widely investigated using electrochemical techniques (Ref 13–16), while published works concerning on this topic of aluminum alloys are rather scarce (Ref 8, 17, 18). Liu (Ref 8) investigated the influence of native oxide and corrosion products on atmospheric corrosion of pure Al through electrochemical impendence spectroscopy (EIS). They revealed that the main influencing factors of native oxide and corrosion products on atmospheric corrosion were structure and thickness. Loose corrosion product layer allowed diffusion of corrosive ions and its protectiveness enhanced with the increase of thickness. However, the relationship between the electrochemical results and the weight loss or corrosion rate data has not been established.

In this work, corrosion behavior of 7A04 aluminum alloy exposed in a tropical marine atmosphere for 4 years was investigated. The corrosion rate was determined by the weight loss method. The composition, structure, and protectiveness of the corrosion products were characterized with microscopic analysis and EIS. The corrosion kinetics, the protective nature of the corrosion products, and the corrosion mechanism of this alloy in tropical marine atmosphere were discussed.

Z.Y. Cui, X.G. Li, C. Man, K. Xiao, C.F. Dong, and **Z.Y. Liu**, Corrosion and Protection Center, University of Science and Technology Beijing, Beijing 100083, China; and **Z.Y. Cui** and **X.Wang**, Institute of Materials Science and Engineering, Ocean University of China, Qingdao 266100, China. Contact e-mail: lixiaogang@ustb.edu.cn.

2. Experimental

2.1 Material Preparation

The materials used in this study were 7A04 aluminum alloy. Chemical composition of this alloy is listed in Table 1. Samples were wet ground through successive grades of silicon carbide abrasive papers from P120 to P2000 followed by diamond finishing to 0.1 μm. Then the specimen was subjected to a scanning electron microscope (SEM, Quanta 250) to observe the distribution and composition of the second phases. For metallographic characterization, the polished surface was further etched using Keller's reagent with the following composition: 1 ml hydrofluoric acid (HF), 1.5 ml hydrochloric acid (HCl), 2.5 ml nitric acid (HNO_3), and 95 ml water (H_2O). After ultrasonic cleaning in ethanol for 1 min and drying in air, the samples were taken immediately to a KEYENCE VHX2000 stereology microscope for microstructure observation. The microstructure of the 7A04 alloy was further investigated by transmission electron microscopy (TEM; TECNAI G^2 F20), with a work function of 300 kV. Thin foils for TEM were cut to about 500 μm by an electron discharge cutter and later ground and polished on both sides to a thickness of about 70 μm. Then the thin foils were ion milled at room temperature in a Gatan PIPS with a small incident angle until perforation.

Figure 1 shows the optical micrograph of 7A04 aluminum. The grain size of this alloy varied between 20 and 200 μm with some coarse and dense intermetallic (IM) particles located on the surface. Figure 1(b) showed the typical microstructure of 7A04 alloy viewed with SEM (in backscattered electron mode), indicating the existence of constituent type particles. The composition of the IM particles in 7××× series aluminum alloys has been investigated by many researchers (Ref 19–21). In general, two kinds of phases were observed: one is the Al-Cu-Fe phase and the other is $MgZn_2$ (η phase). In this work, the Al-Cu-Fe phase, which was always identified as Al_7Cu_2Fe, was detected by energy dispersive spectroscopy (EDS) technique in 7A04 alloy. The Mg-Si particles were also observed as Mg_2Si phases. However, the sub-micron η phase particles were not resolved with SEM.

Figure 2 shows the TEM images of the IM particles and the precipitate-free zone (PFZ) along the grain boundaries in 7A04 aluminum alloy. Fine hardening precipitates were evident along the grain boundaries. The compositions of these particles were determined by Nano-EDS and identified as $Mg(ZnCuAl)_2$, which the $MgZn_2$ precipitates with considerable solubility of Cu and Al (22). The PFZ was about 30-60 nm on either side of the boundary, in which Zn and Cu depletions were expected.

2.2 Field Exposure Test

Samples with the dimension of 100 mm × 50 mm × 2.5 mm were used for field exposure test. Prior to the test, all the specimens were ground down to 800 grit and then degreased by acetone followed by cleaning in ethanol. All the specimens were weighed (original weight) and the surface area (S) was measured before test. Then all the specimens were installed on a test rack with an inclination angle of 45° horizontal to the sky and facing south in Xisha islands (112°20′E, 16°50′N), 100 meters from the coastline. The test duration was 4 years. Four replicate metal samples were retrieved from the exposure site after 1, 3, 6, 9, 12, 24, and 48 months. Three replicas were employed to determine the weight loss of the specimens, and the other one was used to analyze the corrosion morphology and corrosion products.

Table 2 lists the environmental parameters and atmospheric pollutants measured at Xisha Islands during the exposure, which is consistent with the description in our previous work (Ref 23). The average temperature in Xisha marine atmosphere was 27 °C with the maximum temperature increasing up to 33.3 °C and the minimum temperature reducing to 20.1 °C which was also a relatively high temperature. The extreme relative humidity (RH) values oscillated between 61 and 94% with a mean value of 77%. Time of wetness (TOW), which was defined as the period during which a metallic surface was covered by adsorptive and/or liquid film of electrolyte, was another important factor that affects the corrosion behavior of metals in atmosphere. Schindelholz (Ref 24) summarized that the TOW determination methods represented in literature and practice could be categorized by the way in which TOW was treated—either as an environmental parameter or as a surface parameter. However, both methods, ISO 9223 (Ref 25) and other indirect electrode sensors have their limitations (Ref 26–28). In this work, the TOW was treated as an environmental parameter and was calculated according to ISO 9223 (Ref 25), which defines TOW as the time during which the RH of the ambient environment is greater than 80% at temperatures above 0 °C. With this method, the approximate TOW in Xisha islands was 2562 h/year which belonged to the classification of τ_4 (Ref 25). This was a high level due to the high humidity of the tropical marine environment (Ref 29). As for the corrosive species precipitated on the samples, the Cl^- and SO_2 deposition rates were considered and measured using the method given by ISO 9225 (Ref 30). The Cl^- deposition rate was determined by the wet candle method and the SO_2 deposition rate was determined using alkaline surfaces of porous filter plates saturated by a solution of sodium carbonate. The results showed that the annual average deposition rate of chloride was 112.68 mg/m^2 days, which was classified to the S_2, a severe degree with a Cl^- deposition rate between 60 and 300 mg/m^2 days (Ref 25). The precipitation of SO_2 was less than 0.1 mg/m^2 days and the rain had a near-neutral pH of 6.5 because no heavy industry existed at the exposure site.

2.3 Weight Loss Measurement

Corrosion products of the withdrawn triplicate specimens were chemically removed by pickling in the solution (50 mL H_3PO_4 + 20 g CrO_3 + 1L H_2O) for 10 min at 80-100 °C. After that, the specimens were rinsed with distilled water, dried in

Table 1 Chemical composition of 7A04 aluminum alloy used in this work

	Chemical composition (wt.%)							
Alloy	**Si**	**Fe**	**Cu**	**Mn**	**Mg**	**Zn**	**Ti**	**Al**
7A04	0.068	0.42	1.51	0.24	2.62	5.99	0.015	Bal

Table 2 Climatic parameters and atmospheric pollutants of Xisha Islands during 4 years exposure

Exposure site	Location	Max. temperature	Min. temperature	Average temperature	Max. RH	Min. RH	Average RH
XiSha	112°20′E, 16°50′N	33.3 °C	20.1 °C	27 °C	94%	61%	77%
TOW (h/year)	Rain (mm/year)	Cl^- deposition rate (mg/m^2 days)	SO_2 deposition rate (mg/m^2 days)	Sunshine (h/year)	pH of rain	Distance to sea	
2562 (τ_4)	1526	112.68 (S_2)	<0.1 (P_0)	2675	6.5	100 m	

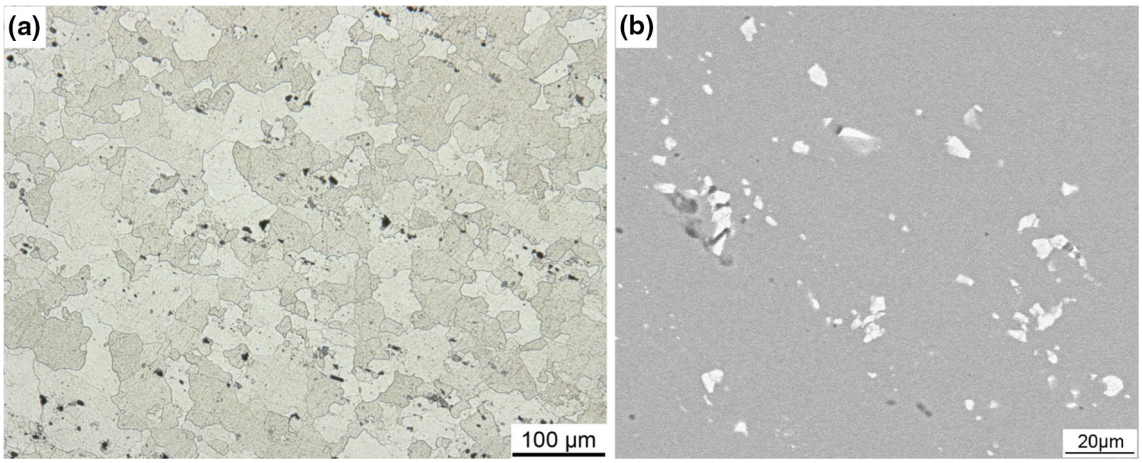

Fig. 1 Microstructure of 7A04 aluminum alloy used in this work: (a) optical micrograph, (b) distribution of the second phases observed by SEM (the white and dark particles are the second phases)

warm air, and then weighed to obtain their final weights (w_1). The weight loss was calculated as follows:

$$C = \frac{w_0 - w_1}{S}, \quad \text{(Eq 1)}$$

where C was the weight loss of the metal due to corrosion (g/m^2), w_0 was the original weight (g), w_1 was the final weight (g), and S was the surface area (m^2). The average corrosion rate after exposure for different periods was calculated by using the equation in Ref 16:

$$V_n = \frac{12(w_n - w_{n-1})}{t_n - t_{n-1}}, \quad \text{(Eq 2)}$$

where V_n was the corrosion rate (g/m^2 year), w_n was the weight loss (g/m^2), t was the exposure time (month), n was the period of exposure (n = 1, 2, 3, 4, 5, 6, and 7 referred to the sample exposed for 1, 3, 6, s9, 12, 24, and 48 months, respectively).

2.4 Characterization of Corrosion Morphology and Corrosion Products

The corrosion morphologies of the exposed samples with and without corrosion products were observed by scanning electron microscope (SEM, Quanta 250). Phase identification was determined by x-ray diffraction (XRD, Rigaku Dmax-rc) and analyzed with Jade 5.0 software.

2.5 Electrochemical Impendence Spectroscopy (EIS) Measurement

EIS measurements were performed with VMP3 electrochemical workstation in 0.1 M NaCl solution in a conventional three-electrode cell, using a platinum sheet as counter electrode and a saturated calomel electrode (SCE) as reference electrode. The test system was always in a steady state with no stirring. The whole metal sample was manually sectioned into coupons of dimensions 15 mm × 15 mm × 2.5 mm which served as working electrode. The working electrode surface was covered with silicone rubber to leave an exposed area of 1.0 cm^2. The impendence spectra were recorded in the frequency range between 100 kHz and 10 mHz with 10 mV amplitude perturbation signal. The experimental data were analyzed by the commercial software ZsimpWin. All the measurements were performed at ambient temperature (25 ± 2 °C) and repeated at least three times to maintain the reproducibility.

3. Results

3.1 Weight Loss and Corrosion Rate

Figure 3 shows the weight loss (a) and the corrosion rate (b) of 7A04 aluminum alloy during the 4-year exposure in Xisha marine atmosphere. The weight loss increases rapidly during the initial 12 months of exposure, followed by a nearly constant

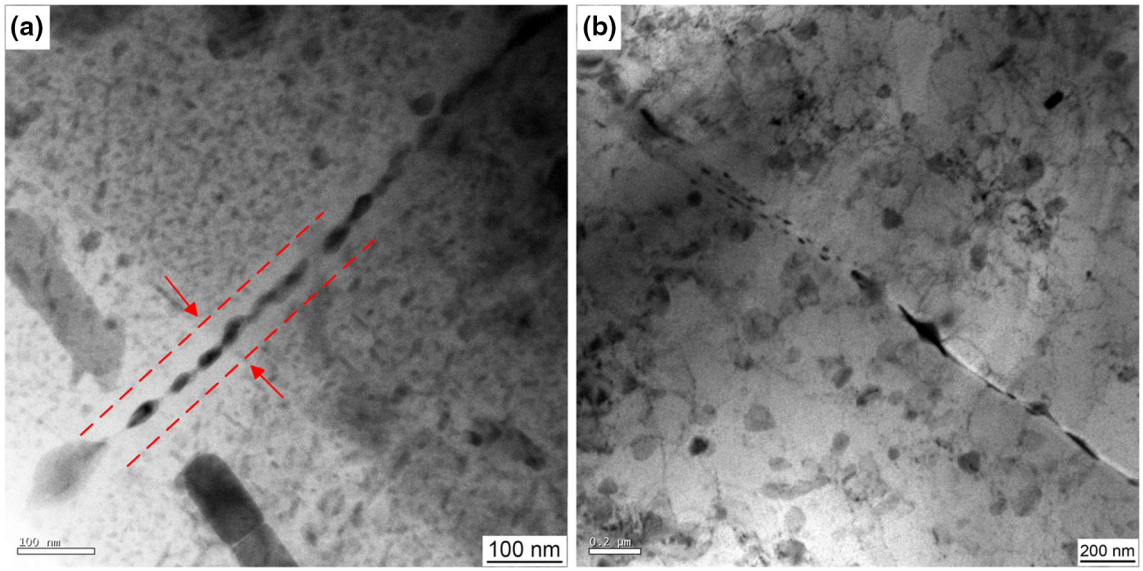

Fig. 2 TEM images of the precipitate-free zone (a) and intermetallic precipitates along the grain boundaries (a and b)

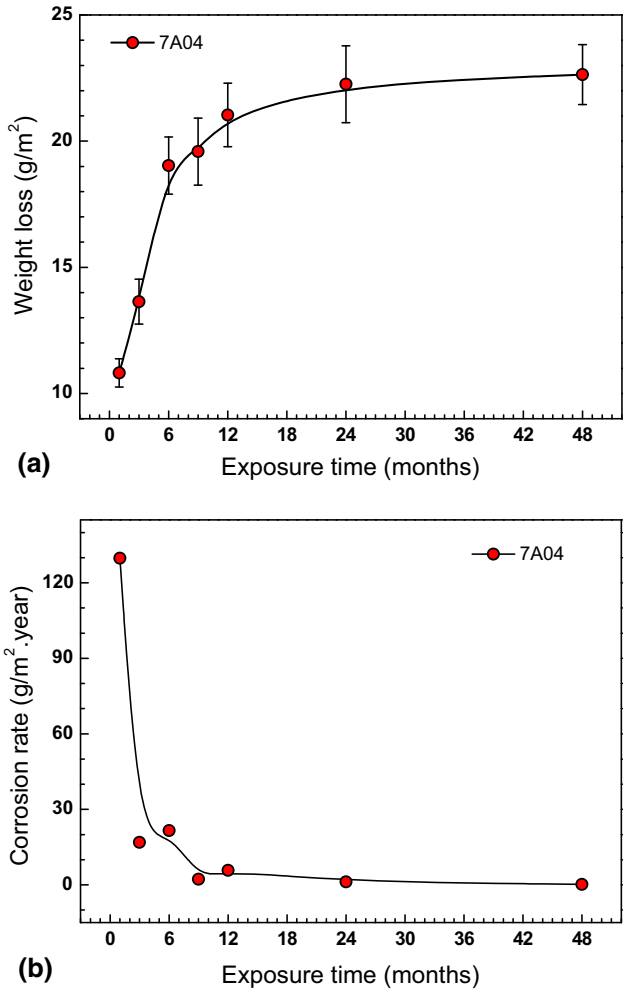

Fig. 3 Weight loss (a) and corrosion rate (b) of 7A04 aluminum alloy during exposure in Xisha marine atmosphere for 4 years, the corrosion rate is calculated by Eq 2

value until the end of the test. Corrosion rate exhibits the maximum value at the first 1 month and then decreases remarkably during the next two exposure months. As the exposure time extends from 3 to 12 months, corrosion rate presents a significant fluctuation. With further increasing of the weathering time, corrosion rate decreases gradually and stabilizes to a certain value. Classification of corrosivity based on corrosion rate measurements of standard specimens according to ISO 9223 has been used in atmospheric corrosion of aluminum in some studies (Ref 9, 31, 32). In Xisha islands, the corrosion rate of 7A04 alloy after exposure for 1 year is 21.03 g/m^2 year, which belongs to the classification of C_5 (very high) based on ISO 9223 (Ref 25).

3.2 Corrosion Product Analysis

3.2.1 SEM Observation. Figure 4 shows the surface morphologies of the corrosion products formed on 7A04 aluminum alloy after exposure for different time periods. It is seen that microcracks are present on the corrosion products after exposure for only 1 month (Fig. 4a) which is mainly attributed to the dehydration process during the wet-dry cycles. With increasing of the exposure time, corrosion product layer becomes more continuous and adherent as shown in Fig. 4(b and c).

3.2.2 Cross-Sectional Morphology. Figure 5 shows the cross-sectional morphologies of the corrosion product layer formed on 7A04 aluminum alloy during the exposure test. A layer of corrosion product generated on the specimen surface during the exposure test. It is worth noting that the substrate corrodes severely at the area which was separated from the corrosion product layer by an uncorroded region. The isolated corrosion zones show an elongated shape or a wide area full of corrosion products among which there exist some cracks. With increasing of the exposure time, the insular corrosion areas tend to spread in depth and connect with each other (Fig. 5d). After 48 months of exposure, the non-corroded matrix (shown as red arrows in Fig. 5e) begins to be peeled off due to the wedge forces created by the precipitation of corrosion products, indicating the occurrence of the exfoliation corrosion.

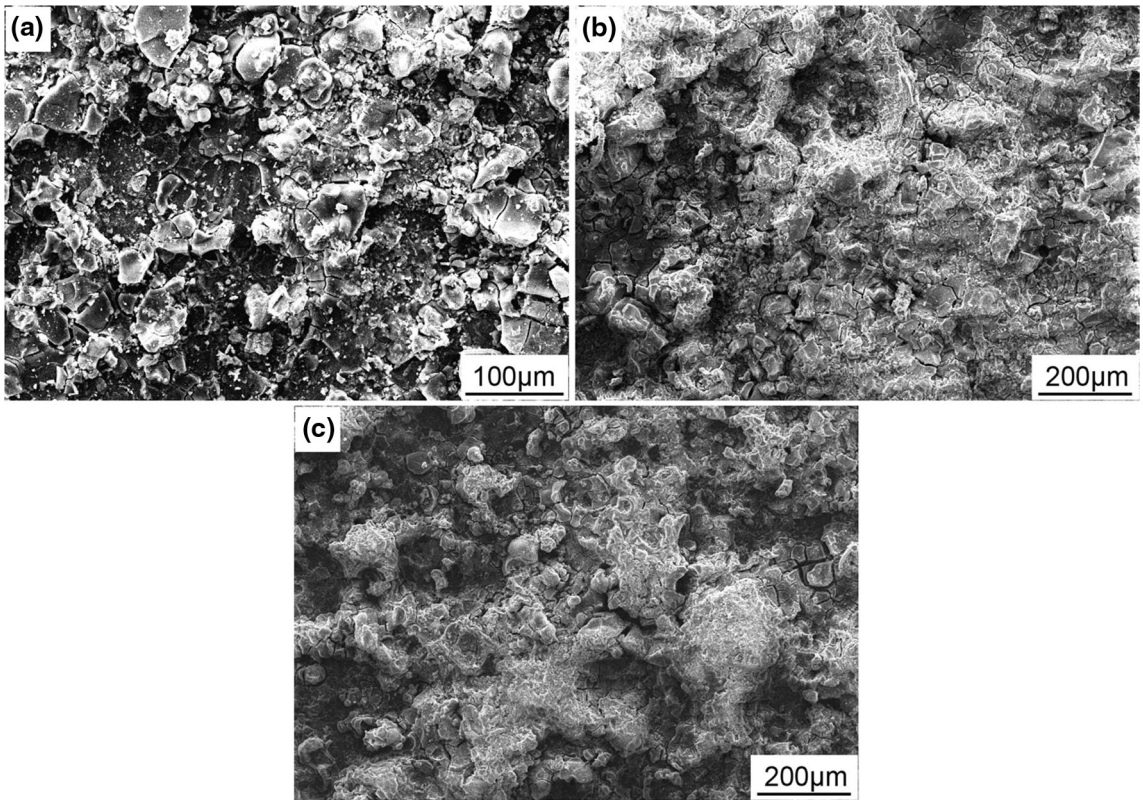

Fig. 4 Surface morphologies of the corrosion products formed on 7A04 aluminum alloy after exposure for 1 month (a), 12 months (b), and 48 months (c)

3.2.3 XRD Analysis. Figure 6 shows the XRD patterns of the corrosion products on the surface of 7A04 alloy after exposure for different time periods. It is obvious that only AlO(OH) is detected during the initial 3 months of exposure. As the exposure test increases up to 6 months, two emerging diffraction peaks around $2\theta = 18°$ and $2\theta = 20°$, which are identified to be $Al(OH)_3$, are detected.

3.3 EIS Measurements

EIS is an efficient method to study the surface condition of metals and also a powerful tool for evaluating the protectiveness of the corrosion product layer formed on metals (Ref 8, 14–16). EIS of 7A04 aluminum substrate and the samples exposed in the exposure experiment after immersion in 0.1 M NaCl for different time periods are shown in Fig. 7. The impedance spectrum of the 7A04 substrate after immersion for 0.5 h exhibits a capacitive loop in the high frequency range and an inductive loop in the low frequency range (Fig. 7a). It has been reported that the low frequency inductance loop of aluminum alloys in aggressive Cl^- solutions is related to the pitting processes (Ref 33, 34). With increasing of the immersion time, the inductive loop disappears and two time constants in impendence diagrams appear. In this stage, it can be speculated that a protective layer forms on the specimen surface and generates a capacitive loop in the high frequency, while the inductive loop is transformed into a second arc which is more directly related to the transfer of charges across the interface (Fig. 7a). As for the product-covered specimens, the inductive loops are only observed on the samples exposed for 1 month (Fig. 7b) and 6 months (Fig. 7c). All of the rest spectra consist of two capacitive loops.

The equivalent circuit models in Fig. 8 are used for fitting the EIS data in Fig. 7. Among them, Model A is used to fit the spectra with two capacitive loops and Model B is utilized for fitting the spectra with inductive loops. In Model A, R_s is solution resistance, CPE_f and R_f are the constant phase element of corrosion product layer and its resistance, and CPE_{dl} and R_t are the double layer capacitance and the charge transfer resistance, respectively. In Model B, the L and R_L are inductance and resistance which represent the initiation of pitting corrosion. The fitting results are shown as solid lines in Fig. 7. It is seen that the equivalent circuits fit the experimental data well in most of the frequency range, which indicates that the equivalent circuits in Fig. 8 are suitable.

The polarization resistance R_p is an important parameter which is proportional to the corrosion rate (Ref 16, 35). R_p can be calculated from the equivalent circuits as follows:

$$\text{Model A}: R_p = R_f + R_t, \quad \text{(Eq 3)}$$

$$\text{Model B}: R_p = \frac{R_t R_L}{R_t + R_L}. \quad \text{(Eq 4)}$$

The R_p of 7A04 alloy as well as the corroded samples during the immersion test is shown in Fig. 9. It is seen that the R_p of the corroded specimens exhibit higher values than that of the freshly prepared sample after immersion for 0.5 h. With increasing of the immersion time, the specimens exposed for 12 and 24 months display higher R_p through the immersion test, while the samples after exposure for 1 and 6 months show

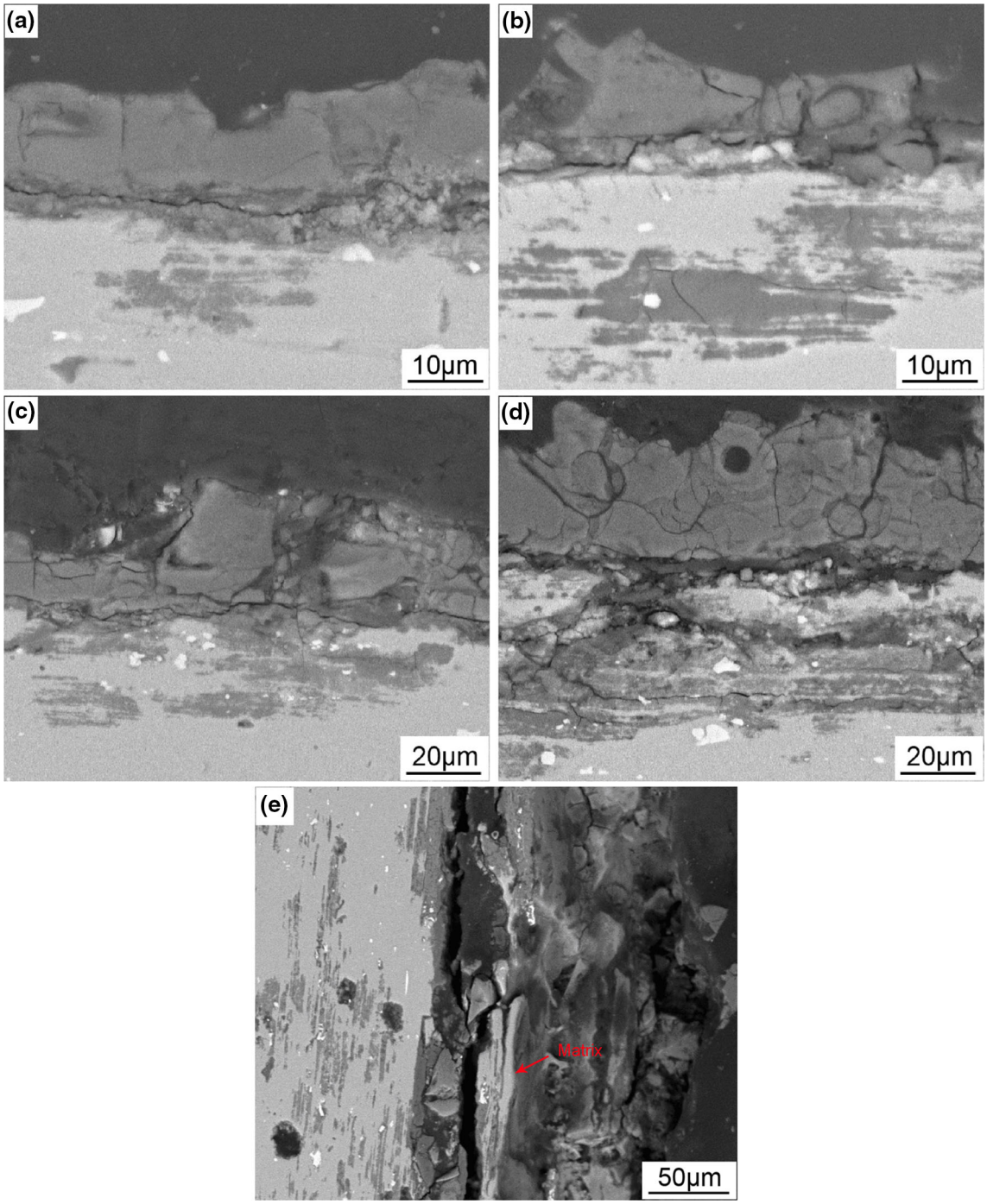

Fig. 5 Cross-sectional morphologies of 7A04 aluminum alloy after exposure for 1 month (a), 6 months (b), 12 months (c), 24 months (d), and 48 months (e)

a similar value with the 7A04 substrate after immersion in Cl^- medium for only 6 h.

3.4 Surface Morphology

The surface corrosion morphologies of 7A04 alloy after removing corrosion products are shown in Fig. 10. It is observed that some pits form on 7A04 alloy after exposure for 1 month (Fig. 10a). As the exposure test extends to 12 months (Fig. 10b), the corrosion sites get deeper and wider, almost covering the whole surface. With further weathering, more grains are corroded away, leaving a rugged surface as shown in Fig. 10c.

3.5 Corrosion Cracks Observation

Figure 11 shows the visual morphologies of the samples exposed for 24 months (a and b) and 48 months (c), which are taken by optical microscope and digital camera, respectively. Some discontinuous cracks, which are parallel to the specimen surface, lie in the middle area of the cross section after exposure for 24 months (Fig. 11a and b). As the exposure is increased to

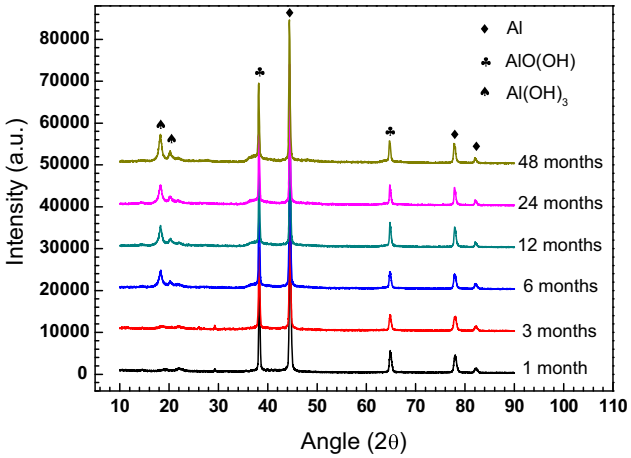

Fig. 6 XRD patterns of the corrosion products formed on 7A04 aluminum alloy after exposure for different time periods

48 months, the cracks beneath the surface grow and become wider, leading to exfoliation as shown in Fig. 11(c), indicating the degradation of the mechanical properties.

Figure 12 shows the optical images of the cracks on the cross section of the specimens after removing the corrosion products and etching with the Keller's reagent. There are many thin, long cracks, which almost penetrate along the grain boundaries throughout the whole specimen. As shown in Fig. 12(a-c), three typical zones are magnified. The first zone near the edge exhibits a wide crack accompanied with some thin cracks (Fig. 12a). Cracks in zone B are thinner than the original wide crack in zone A (Fig. 12b). In zone C, only one discontinuous crack is observed (Fig. 12c).

Figure 13 shows the SEM images of the specimen exposed for 24 months. It is seen that no corrosion product presents in the crack tips. Two typical crack morphologies are detected in Fig. 13: one is the crack with extensive lateral corrosion which is filled with corrosion products (Fig. 13a), the other is the crack penetrated across a grain boundary IM particle which may be caused by the preferential dissolution of the IM particles (Fig. 13b).

4. Discussion

4.1 Corrosion Kinetics of 7A04 Aluminum Alloy in Tropical Marine Atmosphere

4.1.1 Weight Loss Analysis. For aluminum and aluminum alloys, a number of studies have reported the development of corrosion loss with time, both for laboratory investigation (Ref 36, 37) and field exposure test (Ref 4, 6, 7, 9, 38). Most of these studies have interpreted the data in terms of the well-known and widely applied power function (Ref 39):

$$C = At^{n}, \quad \text{(Eq 5)}$$

where C is the weight loss at t years of exposure, A is the weight loss after 1 year exposure, and n is a constant relating to the propensity of the material to corrode. This equation is a simplification of the mathematical result for oxygen diffusion through increasing thickness of the corrosion films. In this paper, however, weight loss of 7A04 alloy is found to deviate from Eq 5. This phenomenon can be easily observed in Fig. 14, which reproduces the result in Fig. 3a by plotting the weight loss against exposure time curves in log-log coordinates. It is seen that the log-log plot of weight loss versus time presents two straight lines taking the 12 month as the turning point. This phenomenon was also observed on 2A12 aluminum alloy in Xisha marine atmosphere in our previous work (Ref 40). The fitting results of the two linear segments are also shown in Fig. 14. It is found that the gradient of the second segment is much smaller than that of the initial segment and both of them are less than 0.5. Firstly, the constant n is a significant parameter that can be considered as an indicator for the physicochemical behavior of the corrosion product layer (Ref 41). Value of n lower than 0.5 suggests a parabolic growth of the layer by formation of protective corrosion products that decrease the corrosion rate by acting as a barrier to the transportation of aggressive agents (Ref 42). In this work, both n_1 and n_2 are less than 0.5 which indicates that a protective corrosion product layer forms on 7A04 aluminum during the exposure test. Secondly, the relatively lower n_2 demonstrates that corrosion products formed on 7A04 aluminum after exposure for 12 months exhibit a better protectiveness, which is confirmed by the EIS results in the following section.

4.1.2 Corrosion Rate Analysis. In general, atmospheric corrosion rate decreases with prolonged exposure time which is attributed to the formation of the protective corrosion product. In this work, as the aluminum alloy is subjected to the tropical marine atmosphere, the chloride ions destroy the surface oxide of aluminum and induce pitting corrosion. With increased exposure time, more and more corrosion products generate on the specimen surface and inhibit the corrosion process. Therefore, a high initial corrosion rate followed by a decreased rate is observed during the initial three months exposure. As the exposure test extends from 3 to 12 months, a significant fluctuation of the corrosion rate is detected in Fig. 3b. This phenomenon is also observed in AZ31 magnesium in the same exposure site (Ref 16) and low carbon steels in tropical marine atmospheres that reported by Ma (Ref 13, 43). Ma (Ref 43) revealed that the corrosion rate in marine environment manifested a so-called "Reverse Phenomenon" in which the average corrosion velocity firstly augmented, and then decreased, and again suddenly increased in a certain period (Ref 13). This special behavior only occurs in marine environment because of the effect of chloride. Therefore, it can be speculated that the fluctuation of the corrosion rate is mainly attributed to the competition between the deterioration effect caused by chloride ions and the stabilization process of the corrosion product layer. As the exposure test continues, corrosion product layer becomes more compact and adherent, i.e., an effective barrier is formed, which results in the situation that the outward diffusion of metallic ions through this layer is rate limiting step. Therefore, the corrosion rate decreases and keeps a steady state until the end.

4.2 Electrochemical Behavior of Corroded 7A04 Aluminum and Its Implication on the Protectiveness of Corrosion Products

It has been generally acknowledged that the presence of chloride ions in environment results in pitting corrosion of Al alloy. Therefore, when the unexposed aluminum alloy is

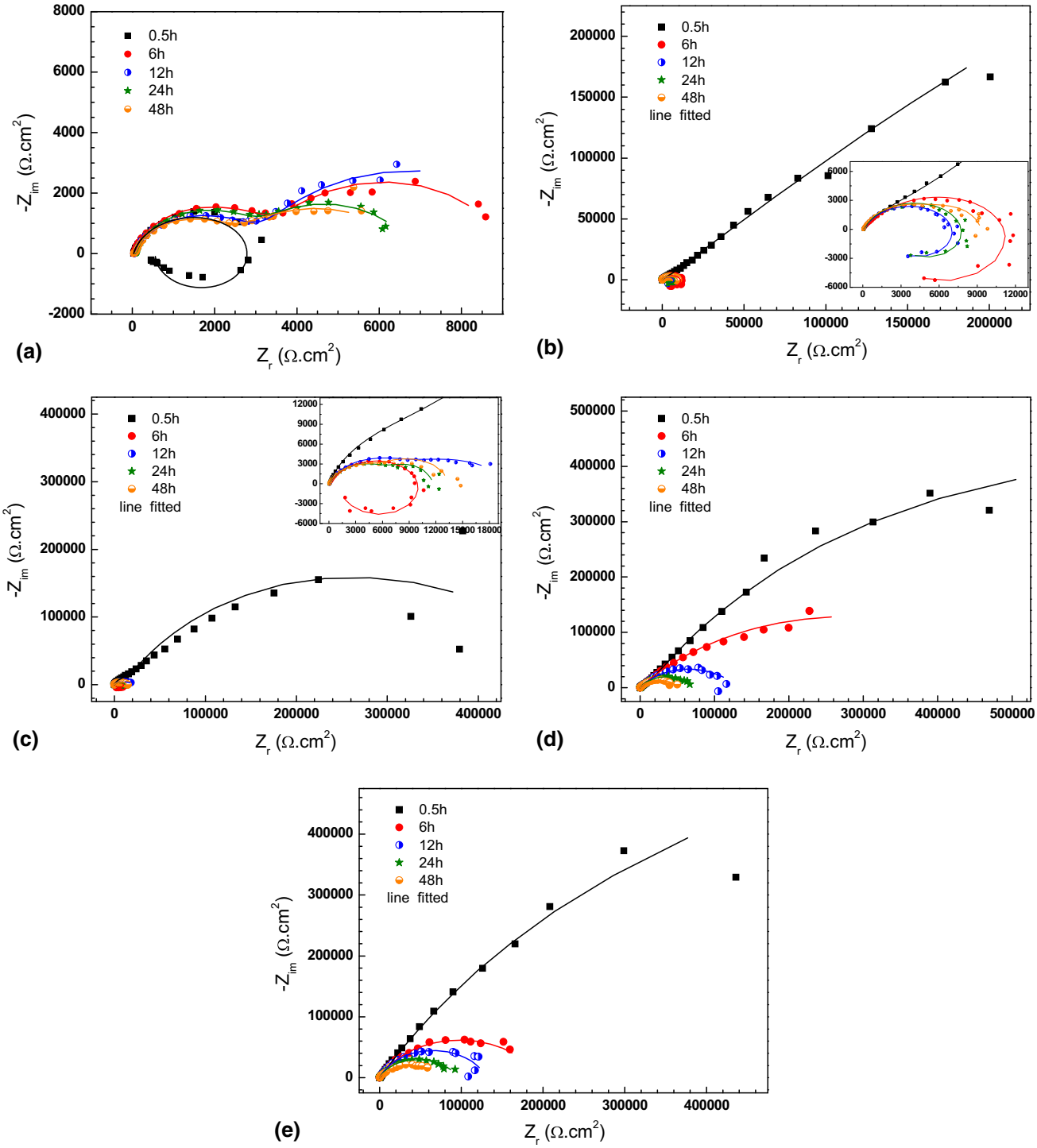

Fig. 7 Nyquist diagrams of 7A04 aluminum alloy substrate (a) and specimens after exposure in the marine atmosphere for 1 month (b), 6 months (c), 12 months (d), and 24 months (e) during the immersion test. The scatter points and the lines are the measured and fitted results, respectively

subjected to immersion in NaCl solution for 0.5 h, pitting corrosion occurs which can be deduced from the inductive loop in Fig. 7a. Scientists demonstrated that inductive behavior is more likely promoted by the weakening of the aluminum oxide layer and occurrence of pitting corrosion due to the anodic dissolution of aluminum alloy (Ref 44). As the immersion test continues, an intact surface layer generates and the inductive loop disappears. For the pre-exposed specimens, the specimen surface is already covered by $Al(OH)_3$ which exhibits barrier effect against corrosion attacks, resulting in the higher R_p and R_f values after immersion for 0.5 h. Simultaneously, Cl^- gives rise to the attack of $Al(OH)_3$ through a slow and stepwise chlorination process, which leads to the localized attack of Cl^- due to the formation of galvanic cell. When the product layer is penetrated, pitting corrosion occurs and an inductive loop appears in the EIS spectra. Therefore, the presence of an

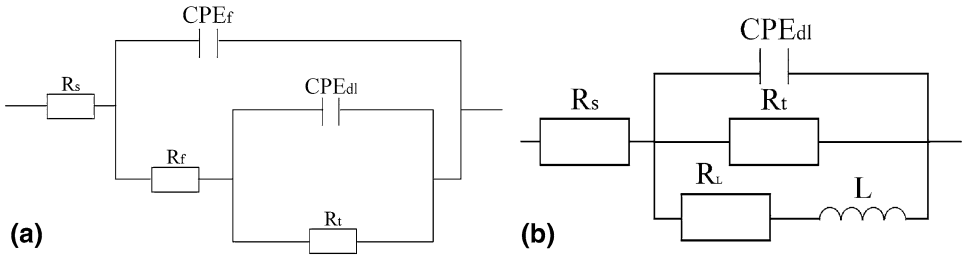

Fig. 8 Equivalent circuits of 7A04 aluminum alloy with different exposure time periods in 0.1 M NaCl: (a) Model A for the spectra with two capacitive arcs; (b) Model B for the spectra with a capacitive loop and an inductive loop

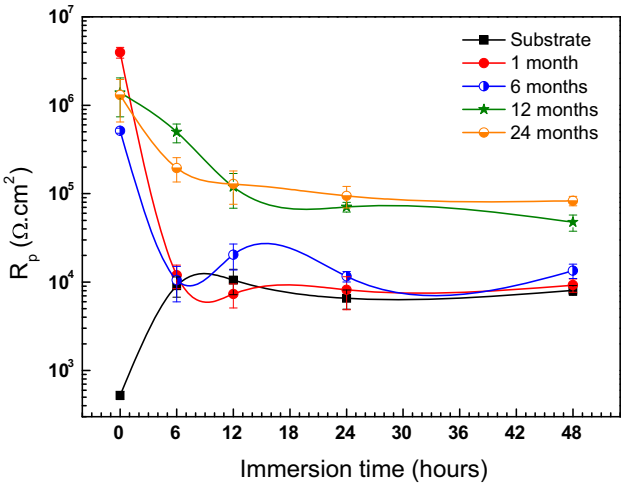

Fig. 9 Calculated polarization resistance (R_p) of the exposed 7A04 aluminum alloy after immersion in NaCl solution for different time periods

inductive loop can be used as an indicator of the state of the product layer, whether or not it is broken. From Fig. 7(b and c), the corrosion film on the specimen exposed for 1 and 6 months remains broken after immersion for 6 h. The difference is that the product layer on the latter specimen is repaired in the following immersion period, while that on the former specimen is repaired after immersion for 48 h. As for the specimens exposed for 12 and 24 months, a continuous layer always exists which can be speculated from the two capacitive loops in Fig. 7(d and e).

On the basis of the above-mentioned analysis, one can find that the corrosion product layers generated on the specimen exposed for 12 and 24 months exhibit good protectiveness against further corrosion attacks. This behavior can also be clearly observed in Fig. 9 in which the R_p values of the two specimens are always higher than the aluminum substrate and the specimens after exposure for 1 and 6 months. This is also the reason why the corrosion weight loss increases slightly during the exposure from 12 to 48 months in Fig. 3(a).

4.3 Corrosion Mechanism of 7A04 Aluminum Alloy in Tropical Marine Atmosphere

In this work, pitting corrosion (Fig. 10), intergranular corrosion (Fig. 12 and 13), and exfoliation corrosion (Fig. 11) are all observed on 7A04 alloy in Xisha tropical marine atmosphere. Pitting caused by chloride attack is one of the most serious forms of corrosion for aluminum alloys and can lead to other types of corrosion as well as structural deterioration. In marine atmosphere, the chloride-containing particles deposited on the aluminum can destroy the surface oxide film of 7A04 alloy and thus induce pitting corrosion. Once the preferential pitting attack occurs on the grain boundaries, intergranular corrosion (IGC) will initiate. It is widely accepted that IGC is caused by the formation of microgalvanic cells between the grain matrix and the grain boundary region, which involved the grain boundary precipitates and the PFZ (Ref 22, 45). In 7A04 aluminum alloy, both grain boundary precipitates and PFZ are detected as shown in Fig. 2. Firstly, η ($MgZn_2$) phases precipitated along the grain boundaries are responsible for the IGC of 7A04 alloy. It has been reported that the η phase has an open circuit potential (OCP) of −1.095 V in 3.5% NaCl solution, which is much lower than that of 7A04 alloy matrix (Ref 46). This overpotential could lead to the preferential dissolution of the anodic particles and formation of the IGC pathways. Secondly, the PFZs next to the grain boundaries also have different electrochemical properties from the grain interior (Ref 22). The segregation of Zn and Mg creates a solute-depleted zone in which the chemical composition is similar to pure Al. Burleigh (Ref 47) has verified that pure Al corroded much faster than the bulk alloy in dilute HCl solution which indicated that IGC of aluminum alloy occurred because the depleted region adjacent to the grain boundaries corroded rapidly in acidic solutions (Ref 47). As the time of exposure increases, the thin networks of intergranular corrosion extend into the material and the fine corrosion pathways thicken and become more pronounced.

With further increase of the exposure time, exfoliation corrosion occurs on 7A04 alloy and the specimen is split down in the middle of the edge area as shown in Fig. 11(c). The mechanism of exfoliation corrosion on high-strength aluminum alloys has been investigated by many researchers (Ref 48–51). A number of factors are believed to play important roles in exfoliation corrosion of aluminum including intergranular corrosion susceptibility (Ref 48, 49), wedge effect on the grain lift-out due to the precipitation of corrosion products (Ref 50), and hydrogen embrittlement (Ref 51). As shown in Fig. 13, it is obvious that there are some corrosion products located along the grain boundaries (Fig. 13a), suggesting that wedge effect from the corrosion products plays a critical role in the exfoliation process of aluminum. In addition, there also exists some thin intergranular corrosion cracks with no evidence of corrosion products (Fig. 13), indicating the possibility of hydrogen effect in the initiation of intergranular cracks. Some previous works have demonstrated that hydrogen was produced from hydrolysis reactions in the anolyte solution at the

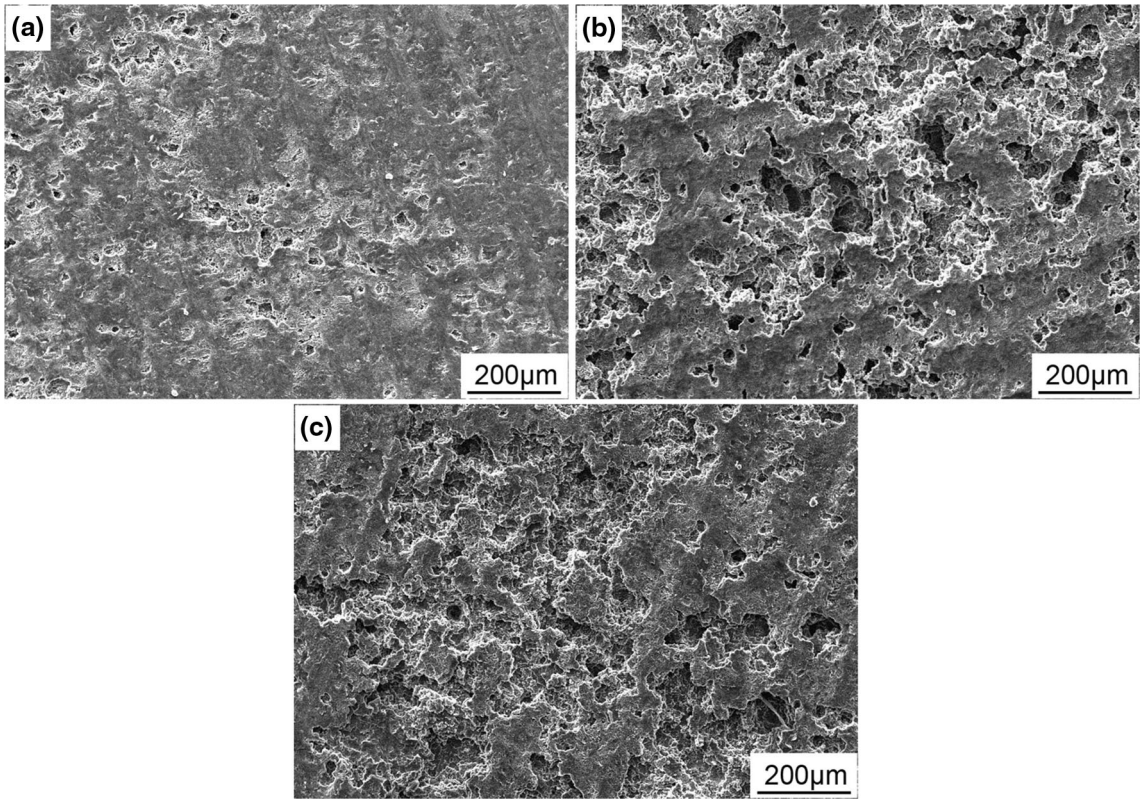

Fig. 10 Surface corrosion morphologies of 7A04 specimens without corrosion products after exposure for 1 month (a), 12 months (b), and 48 months (c)

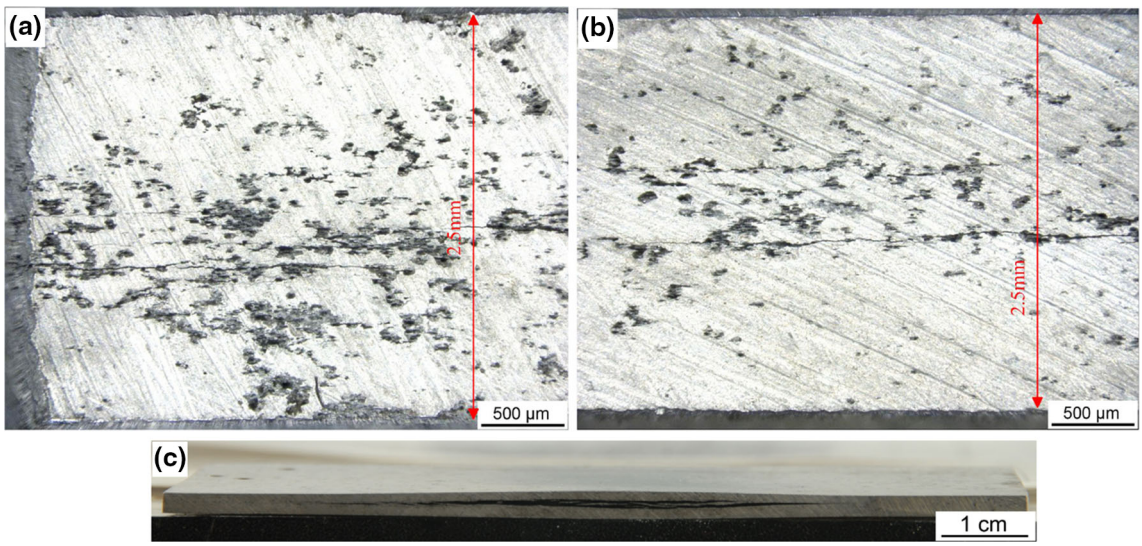

Fig. 11 Cross-sectional morphologies of 7A04 samples exposed for 24 months (a and b) and 48 months (c). For the specimen exposed for 24 months, only microcracks are detected. For the specimen exposed for 48 months, macroscopic cracking occurs in the middle of the specimen

subsurface active corrosion front. It was being trapped in distinct states in the interior of the aluminum alloy and subsequently gave rise to hydrogen embrittlement (Ref 51–53). In marine atmosphere, chloride-containing electrolyte layer absorbed on the surface can easily destroy the surface film to induce pitting corrosion, and finally form occluded cells. Thus, an acidic medium is generated in the corrosion zone due to the hydrolysis of the aluminum cations, accompanying with the hydrogen emissions (Ref 54–56). The formation and molecular recombination of the hydrogen atoms at or close to the grain boundaries generate sufficient pressure to induce crack initiation. Once such cracks initiate, they may propagate extremely fast, creating sudden contact between the aggressive medium and the fresh metallic surface, which in turn, facilitated the

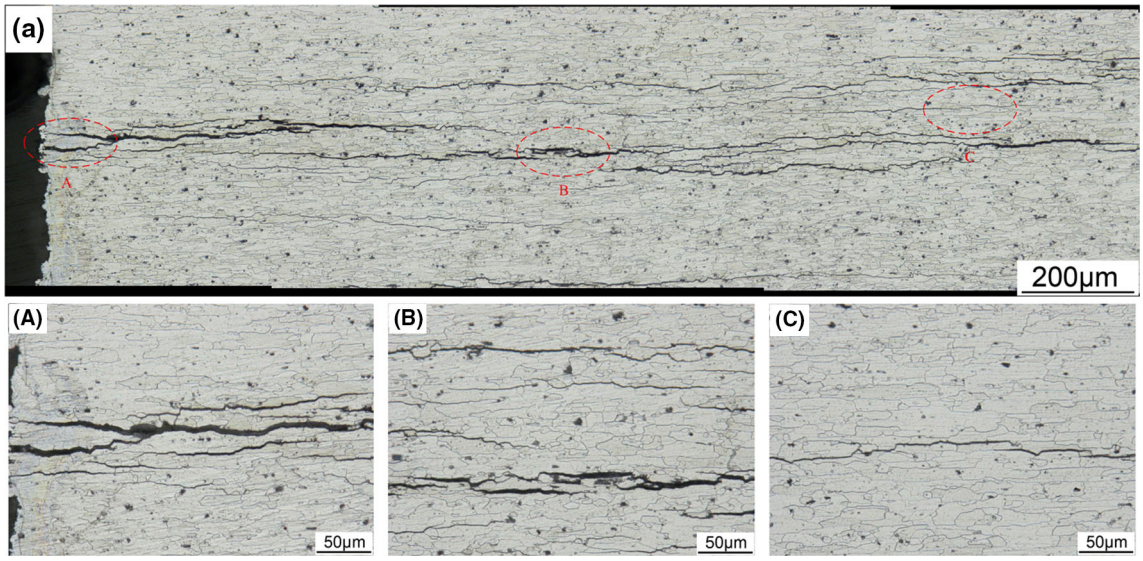

Fig. 12 Cross-sectional crack morphologies of 7A04 alloy exposed for 24 months

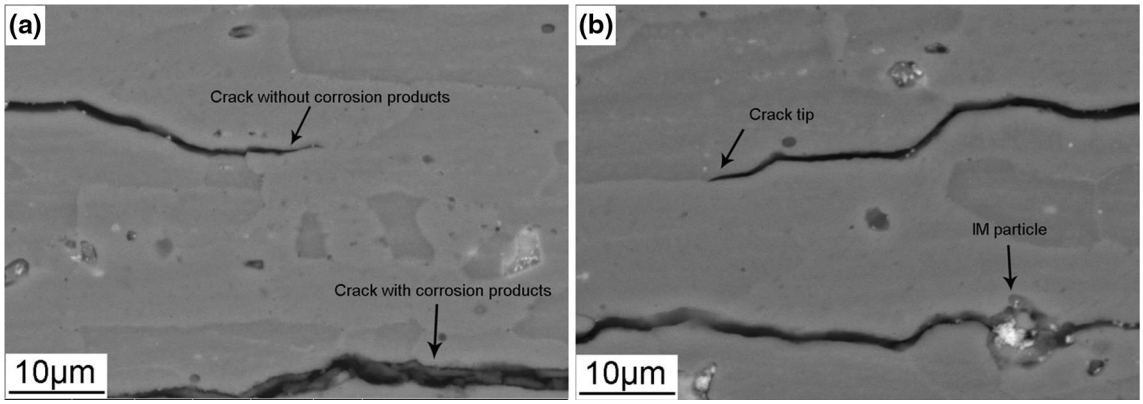

Fig. 13 Crack tip area observation of the 7A04 specimen exposed for 24 months: (a) cracks with and without corrosion products, (b) crack with an IM particle

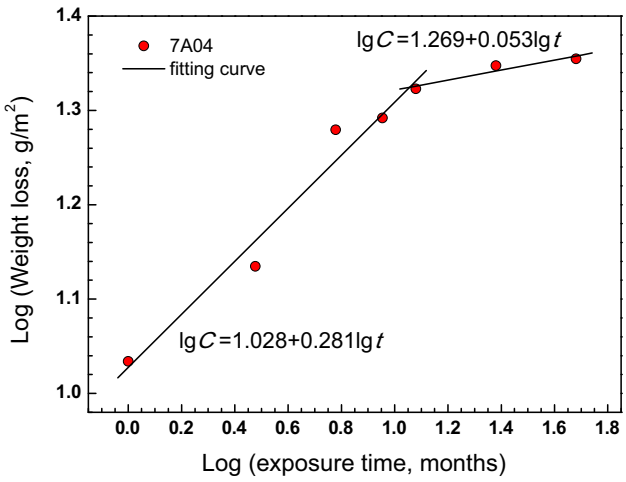

Fig. 14 Bilogarithmic plots of data points from Fig. 3(a) as well as the fitting lines

dissolution of the aluminum substrate. In this case, corrosion products composed of aluminum chloride/oxygen complexes which have higher molar volumes than that of aluminum could form along the gain boundaries. The corrosion products exert a significant wedging pressure between the layers of sheets to pry them apart (Fig. 11c). In conclusion, exfoliation corrosion of 7A04 aluminum alloy in tropical marine atmosphere initiates from hydrogen-assisted intergranular cracks, and then propagates and broadens extensively due to the wedge effect of the corrosion products generated along the grain boundaries.

5. Conclusions

Corrosion behavior of 7A04 aluminum alloy in tropical marine atmosphere was investigated by weight loss calculation, corrosion morphology observation, and electrochemical measurements in this work. The main conclusions were made as follows:

(1) Weight loss of 7A04 aluminum alloy exposed to tropical marine environment deviates from the well-known power-law function: $C = At^n$, but is well fitted with two discontinuous lines in log-log coordinates, taking the 12 months as turning point.
(2) Corrosion rate show a significant fluctuation which is mainly attributed to the competition between the deterioration effect caused by chloride ions and the stabilization process of the corrosion product layer.
(3) The protectiveness of products formed on 7A04 aluminum after atmospheric exposure depends on the exposure time. Corrosion products generated on 7A04 alloy after weathering for 1 and 6 months suppress the corrosion process, while that exposed for 12 and 24 months present better barrier effect against further attacks.
(4) Pitting corrosion, intergranular corrosion, and exfoliation corrosion occur on 7A04 aluminum alloy in the tropical marine atmosphere, indicating a deterioration of the mechanical properties during the exposure.
(5) Exfoliation corrosion of 7A04 aluminum alloy in tropical marine atmosphere initiates from hydrogen-assisted intergranular cracks, and then propagates and broadens extensively due to the wedge effect of the corrosion products generated along the grain boundaries.

Acknowledgment

The authors wish to acknowledge the financial support of the National Basic Research Program of China (973 Program Project, No. 2014CB643300) and the National Science and Technology Basic Project of the Ministry of Science and Technology of China (No. 2012FY113000).

References

1. A. Heinz, A. Haszler, C. Keidel, S. Moldenhauer, R. Benedictus, and W. Miller, Recent Development in Aluminium Alloys for Aerospace Applications, *Mater. Sci. Eng. A*, 2000, **280**, p 102–107
2. T. Dursun and C. Soutis, Recent Developments in Advanced Aircraft Aluminium Alloys, *Mater. Des.*, 2014, **56**, p 862–871
3. S. Knight, M. Salagaras, and A. Trueman, The Study of Intergranular Corrosion in Aircraft Aluminium Alloys using X-ray Tomography, *Corros. Sci.*, 2011, **53**, p 727–734
4. D. De la Fuente, E. Otero-Huerta, and M. Morcillo, Studies of Long-Term Weathering of Aluminium in the Atmosphere, *Corros. Sci.*, 2007, **49**, p 3134–3148
5. T. Li, X.G. Li, C.F. Dong, and Y.F. Cheng, Characterization of Atmospheric Corrosion of 2A12 Aluminum Alloy in Tropical Marine Environment, *J. Mater. Eng. Perform.*, 2010, **19**, p 591–598
6. B. Wang, Z. Wang, W. Han, and W. Ke, Atmospheric Corrosion of Aluminium Alloy 2024-T3 Exposed to Salt Lake Environment in Western China, *Corros. Sci.*, 2012, **59**, p 63–70
7. R. Vera, D. Delgado, and B.M. Rosales, Effect of Atmospheric Pollutants on the Corrosion of High Power Electrical Conductors: Part 1. Aluminium and AA6201 Alloy, *Corros. Sci.*, 2006, **48**, p 2882–2900
8. Y. Liu, Z. Wang, and W. Ke, Study on Influence of Native Oxide and Corrosion Products on Atmospheric Corrosion of Pure Al, *Corros. Sci.*, 2014, **80**, p 169–176
9. S. Sun, Q. Zheng, D. Li, and J. Wen, Long-Term Atmospheric Corrosion Behaviour of Aluminium Alloys 2024 and 7075 in Urban, Coastal and Industrial Environments, *Corros. Sci.*, 2009, **51**, p 719–727
10. S. Sun, Q. Zheng, D. Li, S. Hu, and J. Wen, Exfoliation Corrosion of Extruded 2024-T4 in the Coastal Environments in China, *Corros. Sci.*, 2011, **53**, p 2527–2538
11. D. Sprowls, Evaluation of Exfoliation Corrosion, *ASM Handbook, Corrosion*, Vol 13, L.J. Korb and D.L. Olson, Ed., ASM International, Metals Park, OH, 1987, p 540–543
12. Z. Szklarska-Smialowska, Pitting Corrosion of Aluminum, *Corros. Sci.*, 1999, **41**, p 1743–1767
13. Y. Ma, Y. Li, and F. Wang, Corrosion of Low Carbon Steel in Atmospheric Environments of Different Chloride Content, *Corros. Sci.*, 2009, **51**, p 997–1006
14. J. Wang, Z. Wang, and W. Ke, A Study of the Evolution of Rust on Weathering Steel Submitted to the Qinghai Salt Lake Atmospheric Corrosion, *Mater. Chem. Phys.*, 2013, **139**, p 225–232
15. H. Katayama and S. Kuroda, Long-Term Atmospheric Corrosion Properties of Thermally Sprayed Zn, Al and Zn-Al Coatings Exposed in a Coastal Area, *Corros. Sci.*, 2013, **76**, p 35–41
16. Z.Y. Cui, X.G. Li, K. Xiao, and C.F. Dong, Atmospheric Corrosion of Field-Exposed AZ31 Magnesium in a Tropical Marine Environment, *Corros. Sci.*, 2013, **76**, p 243–256
17. J. Vilche, F. Varela, G. Acuna, E. Codaro, B. Rosales, A. Fernandez, and G. Moriena, A Survey of Argentinean Atmospheric Corrosion: I—Aluminium and Zinc Samples, *Corros. Sci.*, 1995, **37**, p 941–961
18. M. Poltavtseva, A. Heyn, and E. Boese, Long Term Corrosion Behavior of Clad Aluminum Materials Under Different Atmospheric Conditions, *Mater. Corros.*, 2013, **64**, p 723–730
19. A.E. Hughes, N. Birbilis, J. Mol, S. Garcia, X. Zhou, G.E. Thompson, High Strength Al-Alloys: Microstructure, Corrosion and Principles of Protection, *Recent Trends in Processing and Degradation of Aluminium Alloys*, 2011, p 223–262
20. A. Chemin, D. Marques, L. Bisanha, A.D.J. Motheo, W.W. Bose Filho, and C.O.F. Ruchert, Influence of Al_7Cu_2Fe Intermetallic Particles on the Localized Corrosion of High Strength Aluminum Alloys, *Mater. Des.*, 2014, **53**, p 118–123
21. C.B. Fuller, M.W. Mahoney, M. Calabrese, and L. Micona, Evolution of Microstructure and Mechanical Properties in Naturally Aged 7050 and 7075 Al Friction Stir Welds, *Mater. Sci. Eng. A*, 2010, **527**, p 2233–2240
22. T. Ramgopal, P. Gouma, and G. Frankel, Role of Grain-Boundary Precipitates and Solute-Depleted Zone on the Intergranular Corrosion of Aluminum Alloy 7150, *Corrosion*, 2002, **58**, p 687–697
23. Z.Y. Cui, X.G. Li, K. Xiao, C.F. Dong, Z.Y. Liu, and L.W. Wang, Corrosion Behavior of Field-Exposed Zinc in a Tropical Marine Atmosphere, *Corrosion*, 2014, **70**, p 731–748
24. E. Schindelholz, R. Kelly, I. Cole, W. Ganther, and T. Muster, Comparability and accuracy of Time of Wetness Sensing Methods Relevant for Atmospheric Corrosion, *Corros. Sci.*, 2013, **67**, p 233–241
25. ISO 9223, Corrosion of Metals and Alloys—Classification of Corrosivity of Atmospheres, 1992
26. I.S. Cole, W. Ganther, J. Sinclair, D. Lau, and D.A. Paterson, A Study of the Wetting of Metal Surfaces in Order to Understand the Processes Controlling Atmospheric Corrosion, *J. Electrochem. Soc.*, 2004, **151**, p B627–B635
27. I.S. Cole and W. Ganther, Experimental Determination of Duration of Wetness on Metal Surfaces, *Corros. Eng. Sci. Technol.*, 2008, **43**, p 156–162
28. F. Corvo, T. Pérez, Y. Martin, J. Reyes, L. Dzib, J. González-Sánchez, and A. Castañeda, Time of Wetness in Tropical Climate: Considerations on the Estimation of TOW According to ISO 9223 Standard, *Corros. Sci.*, 2008, **50**, p 206–219
29. H. Luo, X. Li, C. Dong, and K. Xiao, Degradation of Austenite Stainless Steel by Atmospheric Exposure in Tropical Marine Environment, *Corros. Eng. Sci. Technol.*, 2013, **48**, p 221–229
30. ISO 9225, Corrosion of Metals and Alloys-Corrosivity of Atmospheres-Measurement of Pollution, 1992
31. T.E. Graedel, Corrosion Mechanisms for Aluminum Exposed to the Atmosphere, *J. Electrochem. Soc.*, 1989, **136**, p 204C–212C
32. Z. Dan, I. Muto, and N. Hara, Effects of Environmental Factors on Atmospheric Corrosion of Aluminium and Its Alloys Under Constant Dew Point Conditions, *Corros. Sci.*, 2012, **57**, p 22–29
33. F. Mansfeld, Models for the Impedance Behavior of Protective Coatings and Cases of Localized Corrosion, *Electrochim. Acta*, 1993, **38**, p 1891–1897
34. B. Wang, L. Zhang, Y. Su, X. Mou, Y. Xiao, and J. Liu, Investigation on the Corrosion Behavior of Aluminum Alloys 3A21 and 7A09 in Chloride Aqueous Solution, *Mater. Des.*, 2013, **50**, p 15–21

35. T. Zhang, Y. Shao, G. Meng, Z. Cui, and F. Wang, Corrosion of Hot Extrusion AZ91 Magnesium Alloy: I-Relation Between the Microstructure and Corrosion Behavior, *Corros. Sci.*, 2011, **53**, p 1960–1968
36. Z.-Y. Wang, T. Ma, W. Han, and G.-C. Yu, Corrosion Behavior on Aluminum Alloy LY12 in Simulated Atmospheric Corrosion Process, *Trans. Nonferr. Met. Soc. China*, 2007, **17**, p 326–334
37. D.B. Blücher, R. Lindström, J. Svensson, and L. Johansson, The effect of CO_2 on the NaCl-Induced Atmospheric Corrosion of Aluminum, *J. Electrochem. Soc.*, 2001, **148**, p B127–B131
38. R.E. Melchers, Bi-Modal Trend in the Long-Term Corrosion of Aluminium Alloys, *Corros. Sci.*, 2014, **82**, p 239–247
39. M. Benarie and F.L. Lipfert, A General Corrosion Function in Terms of Atmospheric Pollutant Concentrations and Rain pH, *Atmos. Environ.*, 1986, **20**, p 1947–1958
40. Z.Y. Cui, X.G. Li, H. Zhang, K. Xiao, C.F. Dong, and Z.Y. Liu, Atmospheric Corrosion Behavior of 2A12 Aluminium Alloy in a Tropical Marine Environment, *Adv. Mater. Sci. Eng.*, 2015, in press
41. D. De la Fuente, I. Díaz, J. Simancas, B. Chico, and M. Morcillo, Long-Term Atmospheric Corrosion of Mild Steel, *Corros. Sci.*, 2011, **53**, p 604–617
42. F. Corvo, C. Haces, N. Betancourt, L. Maldonado, L. Veleva, M. Echeverria, O. De Rincón, and A. Rincón, Atmospheric Corrosivity in the Caribbean Area, *Corros. Sci.*, 1997, **39**, p 823–833
43. Y. Ma, Y. Li, and F. Wang, The Atmospheric Corrosion Kinetics of Low Carbon Steel in a Tropical Marine Environment, *Corros. Sci.*, 2010, **52**, p 1796–1800
44. K. Gopala Krishna, K. Sivaprasad, T. Sankara Narayanan, and K. Hari Kumar, Localized Corrosion of an Ultrafine Grained Al-4Zn-2Mg Alloy Produced by Cryorolling, *Corros. Sci.*, 2012, **60**, p 82–89
45. A.S. El-Amoush, Intergranular Corrosion Behavior of the 7075-T6 Aluminum Alloy Under Different Annealing Conditions, *Mater. Chem. Phys.*, 2011, **126**, p 607–613
46. N. Birbilis and R. Buchheit, Electrochemical Characteristics of Intermetallic Phases in Aluminum Alloys an Experimental Survey and Discussion, *J. Electrochem. Soc.*, 2005, **152**, p B140–B151
47. T. Burleigh, E. Ludwiczak, and R. Petri, Intergranular Corrosion of an Aluminum-Magnesium-Silicon-Copper Alloy, *Corrosion*, 1995, **51**, p 50–55
48. L. Huang, K. Chen, S. Li, and M. Song, Influence of High-Temperature Pre-precipitation on Local Corrosion Behaviors of Al-Zn-Mg Alloy, *Scr. Mater.*, 2007, **56**, p 305–308
49. S. Chen, K. Chen, G. Peng, L. Jia, and P. Dong, Effect of Heat Treatment on Strength, Exfoliation Corrosion and Electrochemical Behavior of 7085 Aluminum Alloy, *Mater. Des.*, 2012, **35**, p 93–98
50. M. Robinson, The Role of Wedging Stresses in the Exfoliation Corrosion of High Strength Aluminium Alloys, *Corros. Sci.*, 1983, **23**, p 887–899
51. H. Kamoutsi, G. Haidemenopoulos, V. Bontozoglou, and S. Pantelakis, Corrosion-Induced Hydrogen Embrittlement in Aluminum Alloy 2024, *Corros. Sci.*, 2006, **48**, p 1209–1224
52. P. Petroyiannis, E. Kamoutsi, A. Kermanidis, S.G. Pantelakis, V. Bontozoglou, and G. Haidemenopoulos, Evidence on the Corrosion-Induced Hydrogen Embrittlement of the 2024 Aluminium Alloy, *Fatigue Fract. Eng. Mater. Struct.*, 2005, **28**, p 565–574
53. T. Zhang, W.Y. Chu, K.W. Gao, and L.J. Qiao, Study of Correlation Between Hydrogen-Induced Stress and Hydrogen Embrittlement, *Mater. Sci. Eng. A*, 2003, **347**, p 291–299
54. T. Marlaud, B. Malki, A. Deschamps, and B. Baroux, Electrochemical Aspects of Exfoliation Corrosion of Aluminium Alloys: The Effects of Heat Treatment, *Corros. Sci.*, 2011, **53**, p 1394–1400
55. T. Marlaud, B. Malki, C. Henon, A. Deschamps, and B. Baroux, Relationship Between Alloy Composition, Microstructure and Exfoliation Corrosion in Al-Zn-Mg-Cu Alloys, *Corros. Sci.*, 2011, **53**, p 3139–3149
56. Z.Y. Cui, X.G. Li, K. Xiao, C.F. Dong, L.W. Wang, D.W. Zhang, and Z.Y. Liu, Exfoliation Corrosion Behavior of 2B06 Aluminum Alloy in a Tropical Marine Atmosphere, *J. Mater. Eng. Perform.*, 2015, **24**, p 296–306